NUMERICAL ANALYSIS OF THE FALL PROCESS AND HAZARD OF SOLID ROCKET MOTOR

Xiaoru JI[1*], Zengyou LIANG[2], Juan LI[3], Bingbing GAO[4]

This study investigates the safety performance of a solid rocket motor subjected to impact loading. A nonlinear finite element method was employed to numerically simulate both the individual-stage drops and the whole-system fall to the ground. Finally, the optimal drop angle at which the motor exhibited no ignition or structural response was identified. Based on the experimental results, the drop response of the whole motor was compared and analyzed. The results show that the first and second stage motors did not respond when they were dropped at different angles. However, the pressure and stress at the bottom of the propellant are larger when falling at 0°, which is more dangerous than other angles. When the motor drops at 30°, 45°and 60°, the nozzles of the secondary motor and the front head of the primary motor do not contact and do not respond. When the whole motor falls 90°, the connecting compartment between the first and second motor is crushed. And the two motors collided. When the whole motor state drops by 60°, the first and second motors show no ignition or deformation response, which is consistent with the simulation results, verifying that the simulation calculation model and parameters are correct. These findings provide valuable guidance for practical applications.

Key words: solid rocket motor; falling risk; numerical simulation; low vulnerability; shock response

1. Introduction

As an energetic material, solid propellant is prone to chemical reaction when exposed to external stimuli. Solid rocket motors face potential accidental stimuli throughout their lifecycle phases, including transportation, maintenance and storage. These stimuli encompass impact events such as free-fall collisions, mechanical shocks, transport vehicle rollovers, and multi-stage rocket launch anomalies. Such incidents pose significant risks to their structural integrity and safety performance,

[1] PhD, School of Mechanical and Electrical Engineering, North University of China, Taiyuan, 030051, China
[2] Xi'an Chang-feng Electromechanical Research Institute, Xi'an, 710000, China
[*]Corresponding author, email: jixiaorujxr@outlook.com
[2] Pro., School of Mechanical and Electrical Engineering, North University of China, Taiyuan, 030051, China
[3] ME, Xi'an Chang-feng Electromechanical Research Institute, Xi'an, 710000, China
[4] ME, Huguan Gaoce New Material Technology Co., Ltd, Changzhi, 047300, China

thereby compromising the overall survivability of the propulsion system.

Ensuring the safety of solid rocket motors under external stimuli has become a major focus of current research [1]. Chen et al. [2] carried out a theoretical analysis of the microstructure of solid propellant [3], studied the damage and failure mode of solid propellant under impact, and established an analysis and calculation model of structural deformation and hot spot formation of solid rocket motor under mechanical impact load. The radial and axial impact tests of small motors were carried out, and the critical impact velocity that caused the formation of high temperature hot spots inside the motor charge was obtained. Wang et al. [4] calculated the critical explosion velocity of a specific size motor radially impacting the steel-soil composite target plate, using a nonlinear finite element dynamics method. Wang et al. [5] analyzed the reaction of a high-energy solid motor of a certain size under the impact load through experiments, established a finite element analysis model for the radial impact target plate of the motor, and judged whether the motor exploded and the location of the detonation point by analyzing the pressure of multiple unit measurement points on the impact surface of the model. Sun and Wang [6] first calculated the response of the high-energy solid rocket motor to impact at different speeds and angles in the radial and axial directions [7], and compared with the experimental results, the accurate numerical calculation model and parameters were obtained. Secondly, the relationship between the size, impact direction and charge of the high-energy solid rocket motor and the impact safety is obtained. In addition, the LS-DYNA was used to numerically calculate the axial and radial impact of the motor, and the critical velocity range of combustion and explosion was obtained.

The safety study of solid rocket motor under impact load can be carried out from three aspects: experiment, theoretical analysis and numerical calculation. Experimental studies are often constrained by site conditions, human factors, and financial limitations, resulting in limited available data [8]. The motor structure is complex, and it is difficult to calculate and analyze it by general analytical theory. Most researchers have studied the safety of solid rocket motors under shock loads through numerical simulation and scaled motor tests [9-12], but these methods have limitations and there is a certain gap with the real motor test. Therefore, this paper uses a combination of numerical simulation and test to study the safety of real solid motors under impact. Numerical calculations are carried out on the fall of the whole motor and its first and second stage motors at different tilt angles. The pressure and stress of the propellant in the motor after the fall were analyzed. Based on the numerical analysis, the drop test of the whole motor is carried out, and the safety angle of the motor drop is optimized, which provides reference value for the engineering application of the motor of this structural type.

2. Simulation model and initial conditions

2.1 Physical Model

The motor and the ground were modeled using Creo software. In order to ensure the reasonable matching of calculation accuracy and calculation speed, some small structures that have little impact on the calculation results are ignored. The simplified model of the motor is shown in **Figure 1**, including the first cabin, the second cabin, the third cabin, the first-stage motor and the second-stage motor.

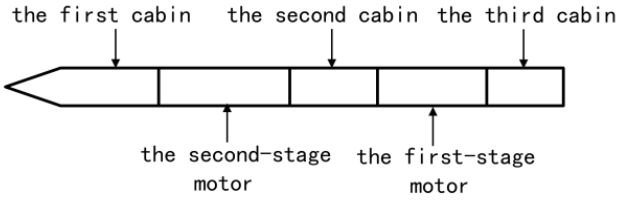

Fig. 1 Simplified model diagram of the entire motor.

The angle between the axis direction and the horizontal ground when the motor is dropped is called the engine tilt 45° (0°, 30°, 60°, 90°) drop angle, as shown in Fig. 2. The motor drop model has symmetry, so the simulation calculation model selects one-half model, as shown in Fig. 3 and Fig. 4. The ground was defined as a rigid body and assumed to be immovable.

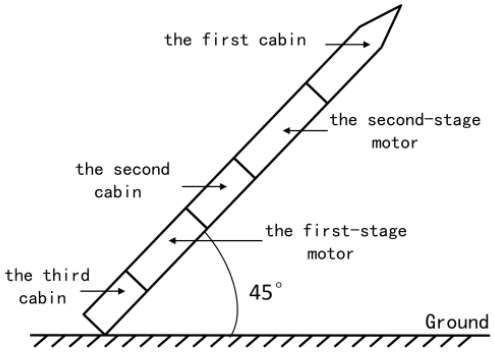

Fig. 2 Motor drop model diagram.

Fig. 3 Simplified model diagram of the first-stage motor.

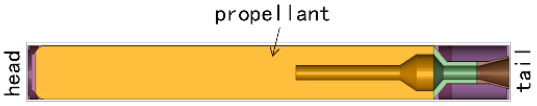

Fig. 4 Simplified model diagram of the second-stage motor.

2.2 Material Model

The housing material of the motor is D406A, and the nozzle material is 2A70-T6. The Johnson-cook constitutive model was used to describe the mechanical behavior of the housing and nozzle materials. The Johnson-cook model [13] is suitable for the calculation of large strain and high strain rate, which can well describe the strain rate of metal materials, and its form is simple, and it has been widely used in the calculation of impact explosion, penetration and other problems.

The constitutive relation expression for the Johnson-cook model is as follows:

$$\sigma_{eq}=\left(A+B\varepsilon_{eq}{}^{n}\right)\left(1+Cln\dot{\varepsilon}_{eq}{}^{*}\right)(1-(T^{*})^{m}) \tag{1}$$

whereσ_{eq} is the yield stress of the material; ε_{eq} is the equivalent plastic strain; $\dot{\varepsilon}_{eq}{}^{*}$ is the dimensionless equivalent plastic strain rate; $T^{*}=(T-T_r)/(T_m-T_r)$is the dimensionless temperature; T is the current temperature, T_r is the room temperature, and T_m is the melting point temperature of the material. A, B, C, m, and n are the static yield stress, the strain hardening modulus, the strain rate correlation coefficient, the strain hardening index, and the temperature correlation coefficient, respectively.

The material properties of each part of the motor are shown in Table 1.

Table 1

Material property

Material	ρ/g▪cm-3	E/GPa	Poisson ratio
Shell	7.85	210	0.3
Propellant	1.78	0.0745	0.498
Nozzle	2.77	69	0.33

The Lee-Tarver ignition growth model [14, 15] and the JWL equation of state [16-18] were used to describe the process of impact initiation of the propellant.

Lee-Tarver ignition growth model：

$$\frac{d\lambda}{dt}=I(1-\lambda)^{b}\left(\frac{\rho}{\rho_0}-1-a\right)^{x}+G_1(1-\lambda)^{c}\lambda^{d}P^{y}+G_2(1-\lambda)^{e}\lambda^{g}P^{z} \tag{2}$$

where the first term on the right side of the equation indicates that part of the propellant is ignited under impact compression. The second term indicates the process of rapid reaction of propellants to produce detonation gas products. The third term indicates the relatively slow process of product diffusion after the main reaction. Where λ is the reactivity of the propellant; t is the time;ρis the density; ρ_0 is the initial density; P is the pressure; I, G_1, G_2, a, b, x, c, d, y, e, g, and z are constants.

JWL Equation of State：

$$p=A\left(1-\frac{\omega}{R_1V}\right)e^{-R_1V}+B\left(1-\frac{\omega}{R_2V}\right)e^{-R_2V}+\frac{\omega E}{V} \tag{3}$$

where p is the pressure of the reaction product; V is the volume of the

reaction product; A, B, R_1, R_2, ω, and E are all parameters that characterize the propellant.

The parameters of the propellant ignition growth model used in the simulation calculations are shown in Table 2. These constitutive and ignition models were implemented in LS-DYNA to perform the numerical simulation. Specifically, the Johnson-Cook model was applied to define the constitutive behavior of the metal shell and nozzle using the MAT_JOHNSON_COOK material keyword. The ignition and reaction behavior of the solid propellant were modeled using the MAT_HIGH_EXPLOSIVE_BURN keyword combined with the EOS_JWL equation of state. This setup allows for a fully coupled simulation of structural deformation and propellant response during the impact process.

Table 2

Parameters of ignition and growth model

I	b	a	x	G1	c	d	y	G2	e	g	z
4.0×105	0.667	0.22	7	800	0.667	1	2	30	0.667	0.667	1

2.3 Parameter Settings

In this paper, ANSYS/LS-DYNA is used for numerical simulation. The constitutive and energetic models described above (Johnson – Cook, Lee – Tarver, and JWL) were embedded in LS-DYNA through the material and equation of state keywords to accurately describe the coupled mechanical and energetic responses of the system. The safety of the first-stage motor and the second-stage motor falling separately under the same conditions was analyzed, as well as the part and degree of interaction between the first-stage motor and the second-stage motor during the fall process of the whole motor. The keyword *CONTACT_AUTOMATIC_SINGLE_SURFACE is used to define the contact between parts and on themselves.

The initial moment of calculation is the moment when the motor is in direct contact with the ground. The drop height of the motor is a fixed value, and the speed (31.6m/s) when it falls to the steel plate can be estimated according to the free fall, and the speed at the moment when the afterbody of the motor touches the ground can be directly given as the motor impact velocity by using the keyword *INITIAL_VELOCITY_GENERATION in the simulation calculation.

3. Simulation results and analysis

3.1 Simulation of the Independent Drop of the First and Second Stage Motors

Figure 5 shows the pressure contour of the propellant during the independent drop process of the first-stage motor at different angles, representing the results discussed in this section. According to Ref. [19], the afterbody of the motor is more dangerous during the fall, so the changes in the afterbody of the propellant during the fall of the motor are analyzed.

Figure 6 shows the pressure and stress time history curves of the monitoring point at the bottom of the propellant of the first-stage motor falling at different angles.

The maximum pressure and stress of the monitoring point of the first and second stage motors dropped at 0°, 30°, 45°, 60° and 90° are shown in Table 3 and Table 4. The peak pressure at the bottom of the propellant in the first-stage motor was 352.95 MPa, 87.92 MPa, 88.04 MPa, 87.98 MPa, and 87.96 MPa, and the stress peaks were 201.46 MPa, 56.23 MPa, 56.21 MPa, 56.22 MPa, and 56.23 MPa, respectively. The peak pressure of the propellant of the second stage motor was 293.55 MPa, 75.50 MPa, 71.12 MPa, 72.33 MPa and 126.51 MPa, and the stress peaks were 200.13 MPa, 152.22 MPa, 134.56 MPa, 126.86 MPa and 141.35 MPa, respectively.

When the first and second stage motors fall separately at 30°, 45°, 60°and 90°respectively. The third cabin is the first to contact with the ground, and different degrees of damage occur. A part of the energy will be consumed. Consequently, the energy transmitted to the propellant is reduced, resulting in lower pressure and stress levels. The drop angles of 30°, 45°, 60° and 90° correspond to relatively low stress values. The difference in stress values is minimal, suggesting that these angles represent the optimal drop conditions.

When the first and second stage motors fall separately at 0°, the third stage is not in direct contact with the ground, so there is no energy consumption. Therefore, the pressure and stress at the bottom of the propellant are the greatest. The large pressure and stress of the propellant indicate that it is subjected to a strong impact effect, and the possibility and number of hot spots generated inside are large, and it is very easy to react, and then cause an accident, so 0°is the relative dangerous fall angle.

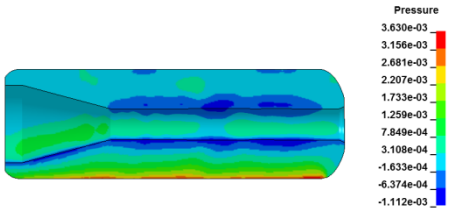

(**a**) 0°

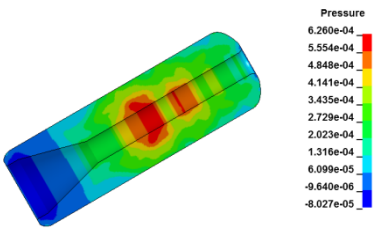

(b) 30°

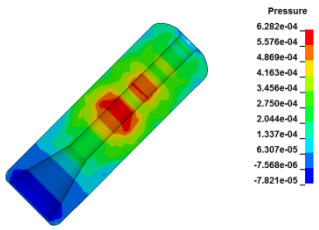

(**c**) 45°

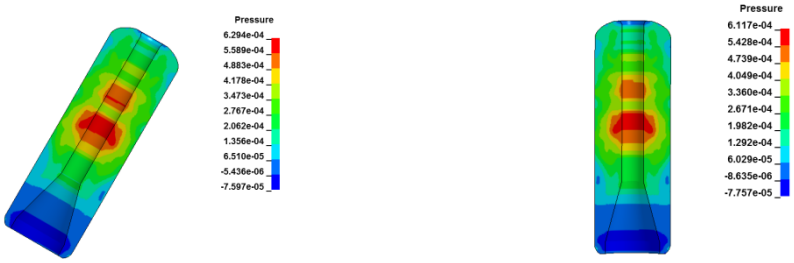

(d) 60° (e) 90°

Fig. 5 Pressure contour maps of the propellant during the first-stage motor drop at different angles (pressure unit: MPa).

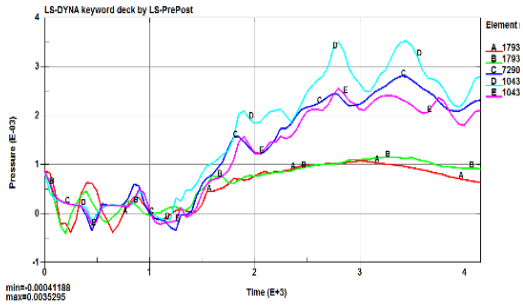

a) curves of pressure-time(0°)

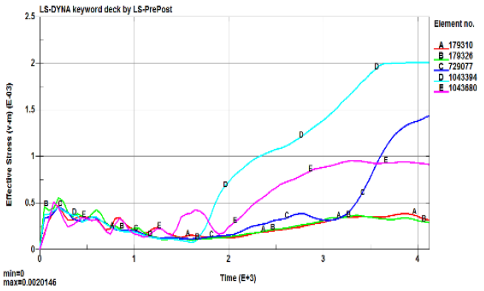

b) curves of stress-time(0°)

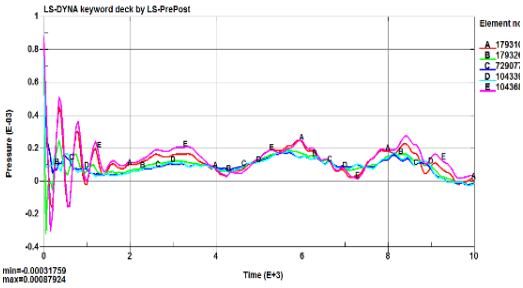

a) curves of pressure-time(30°)

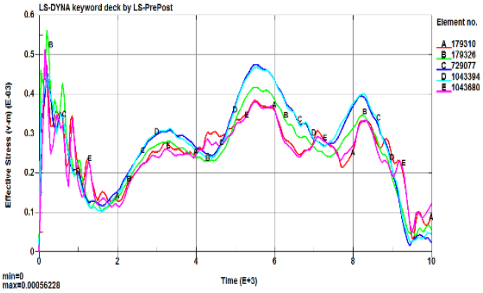

b) curves of stress-time(30°)

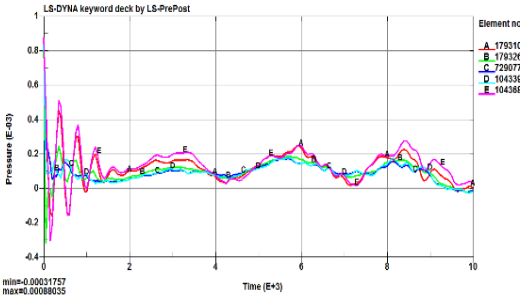

a) curves of pressure-time(45°)

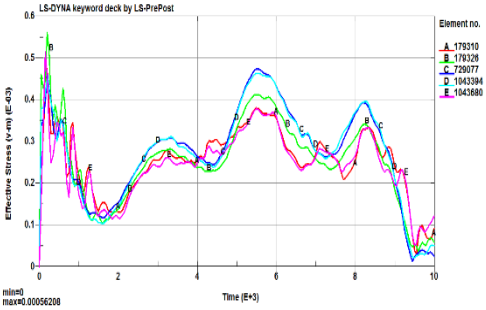

b) curves of stress-time(45°)

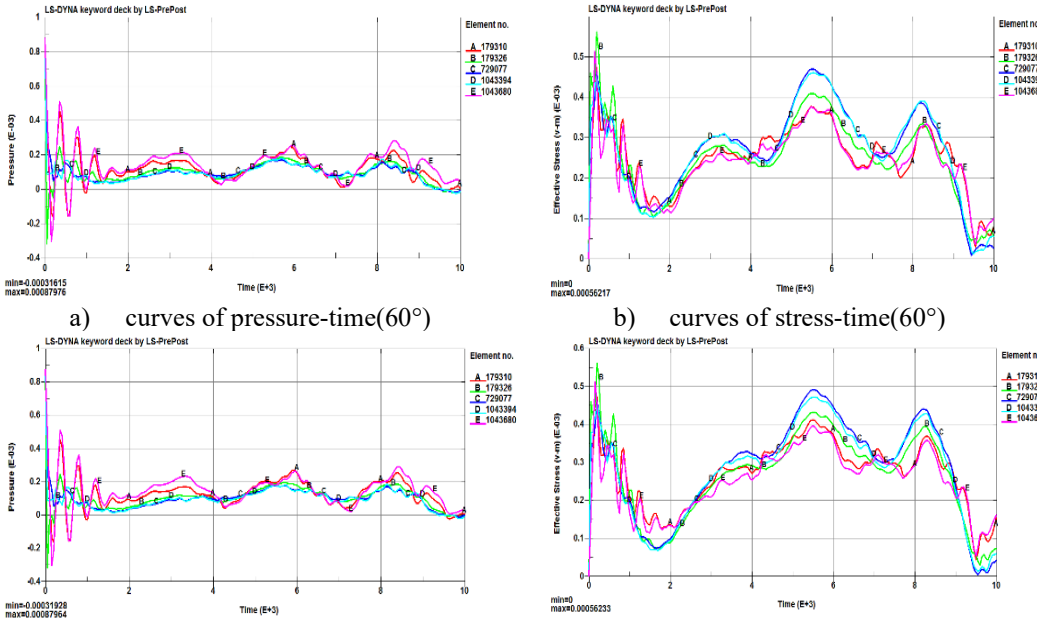

a) curves of pressure-time(60°) b) curves of stress-time(60°)

a) curves of pressure-time(90°) b) curves of stress-time(90°)

Figure 6 Pressure–time and stress–time curves at the bottom of the propellant for different drop angles (pressure and stress in MPa, time in ms).

Table 3

Peak value of propellant pressure and stress when a primary motor drops at different angles

Angle /°	Maximum pressure position of propellant /MPa	Maximum stress position of propellant /MPa
0	352.95	201.46
30	87.92	56.23
45	88.04	56.21
60	87.98	56.22
90	87.96	56.23

Table 4

Peak value of propellant pressure and stress when the second-stage motor drops at different angles

Angle/°	Maximum pressure position of propellant /MPa	Maximum stress position of propellant /MPa
0	293.55	200.13
30	75.50	152.22
45	71.12	134.56
60	72.33	126.86
90	126.51	141.35

3.2 The whole engine is dropped.

The simulations described in Section 3.1 examine the independent drop responses of the first-stage and second-stage motors, focusing on the internal pressure and stress states of each motor when they impact the ground alone. Building on these results, Section 3.2 investigates the coupled dynamic response of the assembled motor during a whole-system drop. The objective is to assess interaction effects between stages that cannot be captured by single-stage simulations, and to evaluate how these interactions influence local deformation, gap evolution, and the potential for propellant ignition.

When the whole motor is dropped at angles of 30°, 45°, 60° and 90°, the fall process is modeled and numerically calculated. **Figure 7** shows the posture of the whole motor drop with the angles of 30°, 45°, 60°and 90°. Table 5 is the distance between the nozzle of the second-stage motor and the front head of the first-stage motor when the whole motor is dropped at different angles.

As can be seen from **Figure 7** and Table 5, when the whole motor is dropped at angles of 30°, 45°and 60°, after the first-stage motor was tipped over, the contact angle between the second-stage motor and the ground did not change significantly. The nozzle of the second-stage motor is not in contact with the front head of the first-stage motor. But as the angle increases, the distance between the nozzle of the second-stage motor and the first-stage motor decreases, and the risk of impact is increased.

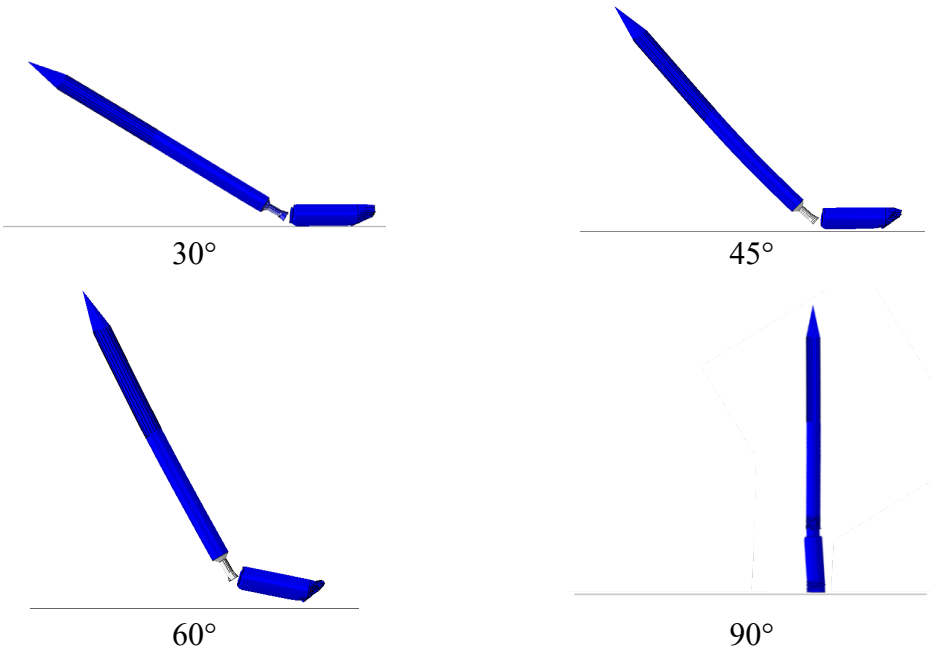

Fig. 7 The entire motor drops at different angles.

Table 5

The distance between primary and secondary motors when the entire motor drops at different angles

Angle/°	The distance between the nozzle of the secondary motor and the front head of the primary motor
30	1.5mm
45	1mm
60	0.4mm
90	0 mm

Fig. 8 is an enlarged diagram of the drop process of the whole motor of 90 °. In the process of the motor dropping, the height h of the connecting compartment between the first motor and the second stage motor decreases with the increase of time. At 8ms, large cracks and small deformations appeared on the connecting cabin. At 16ms, the connecting compartment underwent a huge deformation and some parts were crushed. At 30ms, as the fall continued, the connection compartment was largely crushed. At the same time, the nozzle of the second-stage motor hits the front head of the first-stage motor, causing the front head of the first-stage motor to shear from the weak link. The nozzle of the second-stage motor and the front head of the first-stage motor are inserted into the propellant of the first-stage motor, which causes friction and heat with the local propellant, which may easily lead to the ignition and combustion of the propellant of the first-stage motor. Therefore, when the whole motor is dropped at an angle of 90°, it is a dangerous fall angle..

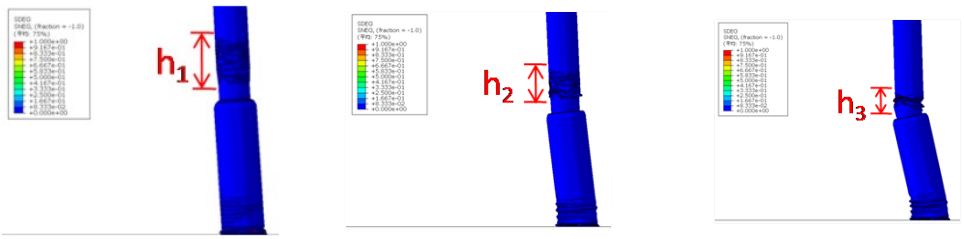

Fig. 8 90 °drop process of the entire motor state.

Sequential deformation process of the whole motor during a drop 90°. The figure shows the progressive crushing of the connecting compartment at 8 ms, 16 ms, and 30 ms. h_1, h_2, and h_3 represent the measured heights of the connecting compartment at these three-time steps, respectively. Through simulation, it can be concluded that during the drop at angles of 0°, 30°, 45°, 60°and 90°. The motor alone at 0° (horizontal) has the highest stress, which is the most dangerous drop angle. The simulation results show that when the whole motor is dropped at 90°, the nozzle of the second-stage motor collides with the front head of the first-stage motor.Under the impact of the propellant of the first and second stage motors, hot spots are generated inside, and hot spots react, which may easily cause accidents.

When dropped at angles of 30°, 45° and 60°, the greater the angle, the smaller the distance between the nozzle of the second-stage motor and the front head of the first-stage motor. The greater the risk of collision between the primary and secondary motors. Compared to 30° and 45°, the entire motor is tilted at 60° and it is more dangerous to fall.

4. Experimental Part

4.1 Test Layout and Process

The engine is attached to the drop frame by a sling. The ground is made up of a concrete base and steel plates. The drop height is the distance between the lowest point of the motor and the ground. The drop test layout is shown in Fig. 9.

During the test, the motor and tooling are securely fixed to the release mechanism and the ground, respectively. After the tester evacuates to a safe position, the motor is lifted to a fixed height and kept stable. The motor is then released by a release mechanism to allow it to fall freely, while a monitoring device is used to record the fall process.

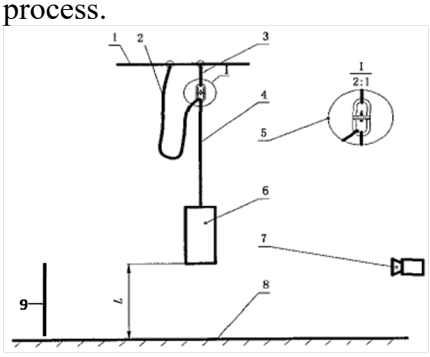

1- Falling frame; 2- Anti-collision rope; 3- Hanging rope (upper); 4- Hanging rope (lower); 5- Release device; 6- Motor; 7- High speed photography equipment; 8- Falling platform; 9- Witness board

Fig. 9 Layout diagram of drop test.

Analysis of Test Results

1) The process of the whole engine dropping.

The drop test of the whole motor height of 48m and inclination of 60°was carried out. During the whole motor drop, the third compartment of the interstage was the first to touch the ground. And the cracks appeared in the connecting compartment between the first and second stage motors. As the fall continued, the connecting compartment was fragmented. And the first stage motor toppled over and hit the ground, followed by the second stage. In the process of dumping of the first-stage motor, the nozzle and connecting compartment of the second-stage motor did not collide with the first-stage motor, and no ignition or significant structural

deformation was observed in either the first-stage or second-stage motors after the test.

2) Overpressure test situation.

The overpressure acquisition is a free-field shock wave overpressure acquisition system with two test points. The test point is 12m away from the landing point. And two overpressure sensors are arranged at each test point. The schematic diagram of the test point layout is shown in Fig. 10.

The range of the four overpressure sensors is 0.35 MPa. And the trigger threshold is set to 0.003 MPa. During the test, none of the 4 sensors was triggered. So none of the sensors collected an overpressure signal. It shows that the overpressure of more than 0.003 MPa is not generated during the drop of the whole motor. After the test, the status of the overpressure sensor was reviewed. And the test performance of the sensor was normal, which ruled out the possibility of damage to the acquisition system. So there was no overpressure in this drop test.

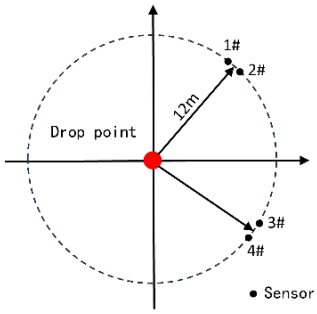

Fig. 10 Layout diagram of overpressure measurement points.

3) Witness the impact of the board.

Witness plates are arranged at three forward azimuth 6m around the drop point of the whole motor. The location of the witness board is shown in Figure 11.

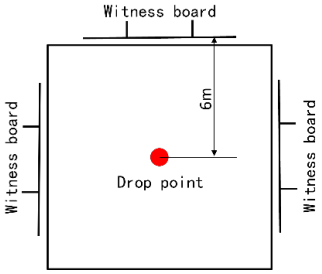

Fig. 11 Witness board layout diagram.

After the engine fell, there were no impact marks on the three witness boards, as shown in Figure 12. After the whole motor is tilted and falls by 60°, the first and second stage motors are unresponsive. And the whole motor is also in a safe state. Therefore, 60° is the safe drop angle of the motor. The experimental results are

consistent with the numerical calculation results, indicating that the accuracy of the numerical simulation model is high.

a) b) c)

Fig. 12 Witness board status diagram after the entire motor falls.

5. Conclusion

The first and second stage motors were simulated and calculated at different tilt angles of 0°, 30°, 45° and 60° and 90°. The results show that the internal pressure and stress of the propellant are the largest when the first and second stage motors are dropped at 0°. A horizontal drop at 0° is therefore the most dangerous angle for the motor.

The whole motor was also simulated and calculated at tilt angles of 30°, 45° and 60° and 90°. When the whole motor is dropped at 90°, there is a high risk that the column of the first-stage engine will be crushed and rubbed, which may lead to ignition and fire. When dropped at 30°, 45° and 60°, the first-stage motor is not subject to crush impact. However, as the drop angle increases, the distance between the secondary motor and the first-stage motor decreases, which raises the potential collision risk.

A 60° drop test was carried out on the whole motor. After the motor fell, no ignition or abnormal deformation occurred, and there was no contact between the first and second stage motors. This result was consistent with the simulation results, confirming the accuracy of the simulation calculation model. Therefore, a tilt angle of 60° can be identified as the safest drop angle.

The measures that can avoid motor accidents in engineering applications include but are not limited to the following two aspects. First, strengthen the connecting compartment between the first and second stage motors to avoid collision between the nozzle of the second stage motor and the first-stage motor. Second, reinforce the casing of the first-stage motor to reduce the risk of rupture. These findings provide valuable guidance for the safe structural design and practical application of solid rocket motors in aerospace engineering.

REFERENCES

[1] *B. Sun*, Numerical simulation study on impact characteristics of solid propellant fragments, PhD Thesis, Academy of Aerospace Propulsion Technology, Xi'an, 2022.
[2] *G. Chen*, Investigation of the safety for solid rocket motor under mechanical impact, PhD Thesis, National University of Defense Technology, Changsha, 2005.
[3] *G. Chen, W. Zhang*, Numerical analysis of SRM's safety under mechanic impact, J. Aerosp. Power, 2006(04): 784–788.
[4] *Y. Wang, J. Lu, L. Chen, L. Chen*, Numerical analysis for safety of solid rocket motor impacting target, J. Solid Rocket Technol., 2009, **32**(03): 274–277+283.
[5] *Y. Wang, K. Liu, L. Sun, K. Li*, Rocket sled experiment and numerical simulate on high energy SRM, J. Solid Rocket Technol., 2014, **37**(06): 873–876.
[6] *Q. Sun, J. Wang*, Numerical analysis of impact safety of solid rocket motor, J. Solid Rocket Technol., 2020, **43**(03): 376–382.
[7] *Q. Sun*, Numerical analysis of impact of solid rocket engine, PhD Thesis, Nanjing Univ. of Sci. and Technol., Nanjing, 2019.
[8] *R. Li, Y. Dang, H. Li, Z. Wang*, Experimental study of the solid rocket motor vulnerability, Missiles Space Veh., 2019(05): 53–58.
[9] *H. Cun, R. Guo, P. Song*, Numerical analysis of safety of solid rocket engine during falling process, Acta Armamentarii, 2018, **39**(S1): 66–71.
[10] *H. Shi, K. Dan, Y. Zhang, Z. Xiang*, Numerical simulation of initiation threshold of solid engine by shaped-charge jet, J. Ordnance Equip. Eng., 2022, **43**(06): 24–28+78.
[11] *C. Wang, G. Xu, Y. Zhu*, Numerical calculation of solid rocket motor drop process, J. Solid Rocket Technol., 2018, **41**(05): 562–565.
[12] *Z. Zhang, X. Shen, Z. Mo, T. Bai*, Numerical research of shock initiation process of SRM with mechanical impact loading, J. Proj. Rockets Missiles Guid., 2022, **42**(03): 55–60.
[13] *G. R. Johnson, W. H. Cook*, A constitutive model and data for metals subjected to large strains, high strain rates and high temperatures, Eng. Fract. Mech., 1983, **21**: 541–548.
[14] *E. L. Lee, C. M. Tarver*, Phenomenological model of shock initiation in heterogeneous explosives, Phys. Fluids, 1980, **23**: 2362–2372.
[15] *C. M. Tarver, J. W. Kury, R. D. Breithaupt*, Detonation waves in triaminotrinitrobenzene, J. Appl. Phys., 1997, **82**(8): 3771–3782.
[16] *S. Lu, W. Luo, W. Chen, W. Wang*, Experiments and numerical simulations of sympathetic detonation of high-energy solid propellant in shell, J. Harbin Eng. Univ., 2014, **35**(12): 1507–1511+1552.
[17] *J. Wu, L. Chen, J. Lu, C. Feng*, Research on shock initiation of the high energy solid propellants, Acta Armamentarii, 2008(11): 1315–1319.
[18] *X. Jiang, X. Long, B. He, L. Chen*, Numerical simulation of detonation in aluminized explosives containing oxidiser (AP), Explosion Shock Waves, 2005(01): 26–30.
[19] *M. Yang, W. Huang, W. Shen, G. Li*, Numerical simulation and experimental analysis of drop at different angle of solid rocket motor, Chin. J. Energetic Mater., 2018, **26**(09): 726–731.